Coordinated Dispatch of Distribution Network and Microgrid via Microgrid Flexible Operation Region Under Aggregated Regulation Cost Constraints

Zhinong Wei, Peng Liu, Sheng Chen, Jingtao Zhao, Shu Zheng, and Guoqiang Sun

Abstract—**To address the limited adjustable capacity of distribution networks (DNs) under the large-scale integration of flexible resources into microgrid (MG), an MG flexible operation region (MGFOR) model is proposed to quantify the adjustability of MG under aggregated regulation cost constraints. A coordinated dispatch framework of DN and MG is then developed based on MGFOR to enable cooperative flexibility allocation. The original boundary of MGFOR is determined through a radial iterative linear search, and its construction is completed using a convex-hull fitting approach. The simulation is conducted on the modified IEEE 33-node test system. It is demonstrated that MGFOR explicitly quantifies adjustable power boundaries, yielding 2.2% lower total operation cost for the proposed coordinated dispatch framework of DN and MG compared with hierarchical dispatch framework of DN and MG. The voltage safety margins at noon are enhanced by up to 56.46% at distribution feeder terminals. Furthermore, the impact of operation modes of distributed photovoltaic units on node voltage in DN is comparatively analyzed.**

Index Terms—**Distribution network, microgrid, coordinated dispatch, convex-hull fitting, demand response, economic dispatch, flexible operation region, aggregated regulation cost constraint.**

I. Introduction

THE goals of global carbon neutrality have accelerated the integration of renewable energy (RE) into power systems. By 2024, RE installations reached 585 GW, representing 92.5% of newly added capacity [1]. With the rapid increase in RE penetration, traditional distribution networks (DNs) have been transformed from passive, one-way systems into active DNs, resulting in heightened operation volatility and security concerns [2]. As a key platform for deploying flexible resources (FRs), microgrids (MGs) enable localized power optimization by integrating RE generation, energy storage system (ESS), and flexible load (FL), thus playing a crucial role in enhancing RE consumption and improving the reliability of power supply [3], [4].

The large-scale integration of MGs results in higher demands on the operation flexibility of DN. Recent studies have explored local solutions such as multi-terminal soft open points to regulate voltage in renewable-rich DNs [5], and demand response (DR) -coupled reconfiguration to improve reliability [6]. While effective for device-level or system-level control, these approaches lack a coordination framework to coordinate the flexibility provision between MGs and the upstream DN. However, the prevailing independent dispatch framework for DN and MG, termed hierarchical dispatch (HD) framework, also faces critical challenges of conflicting optimization objectives, potentially leading to operation efficiency losses and node voltage violation risks in DN due to insufficient adjustable capacity [7], [8]. Crucially, even when coordination is attempted, the prevailing HD framework is not effective in characterizing the true adjustable capacity or flexibility potential of MG for the distribution system operator (DSO). Therefore, the use of extensive FRs within MG for the coordinated dispatch and control of DN, through the establishment of a cross-layer coordinated dispatch framework of DN and MG, presents a promising pathway to address these challenges.

Research on the coordination of DN and MG has primarily focused on modeling approaches and solution algorithms. In the context of game-theoretic frameworks, related modeling approaches can be categorized into two primary branches. Within the framework of cooperative game theory, [9] proposed a cooperative game-based MG alliance agreement and developed a complementary power supply scheme between DN and the alliance, employing the Shapley value to ensure fair benefit distribution. In contrast, within the framework of non-cooperative game theory, [10] proposed a bi-level optimization model integrating two-stage robust optimization to minimize the operation costs of multiple entities in

Manuscript received: May 13, 2025; revised: July 3, 2025; accepted: December 15, 2025. Date of CrossCheck: December 15, 2025. Date of online publication: February 2, 2026.

This work was supported by the Science and Technology Project of State Grid Corporation of China (No. 5400-202340552A-3-2-ZN).

Z. Wei, P. Liu, S. Chen (corresponding author), and G. Sun are with the School of Electrical and Power Engineering, Hohai University, Nanjing 211100, China (e-mail: wznnj@263.net; lp15503912892@163.com; chenshenghhu@163.com; hhusunguoqiang@163.com).

J. Zhao and S. Zheng are with NARI Technology Co., Ltd., Nanjing 211106, China (e-mail: Zhaojingtao@sgepri.sgcc.com.cn; suncau@foxmail.com).

DOI: 10.35833/MPCE.2025.000427

hybrid AC/DC distribution systems with MG clusters under RE uncertainty. In the area of collaborative dispatch algorithms, distributed optimization algorithms are mainstream due to their inherent compatibility with multi-agent decision-making characteristics. Reference [11] proposed a real-time distributed dispatch strategy between low-voltage DNs and medium-voltage MGs, which reduced computational and communication overhead by decoupling internal equipment dispatch from ancillary service optimization. Reference [12] introduced a distributed optimization framework using inverter-based reactive power support and storage flexibility, enabling collaboration among multiple MGs for ancillary services. A fully distributed algorithm based on the alternating direction multiplier approach was employed to preserve individual decision-making autonomy. Reference [13] applied analytical target cascading to solve the hierarchical economic dispatch problem between DN and multi-agent MGs under RE uncertainty. Additionally, reinforcement learning algorithms were applied [14].

Effectively managing the pervasive uncertainties associated with RE generation and load demand is also important for practical coordination of DN and MG. Reference [15] proposed a cooperative day-ahead dispatch approach for DNs and MGs based on chance-constrained programming. A mixed-integer linear programming (MILP) model was constructed using linearization techniques, which minimized operation cost while ensuring frequency stability under high uncertainty conditions. Reference [16] developed a network-constrained transactive control framework with two-timescale optimization to handle uncertainties in the multi-MG-based DN. Beyond routine operation, the coordination of DN and MG holds significant promise for enhancing distribution system resilience, especially during extreme event-induced faults. Reference [17] formulated an MILP model for coordinating interruptible loads across multiple MGs, optimizing their allocation to minimize outage penalties. Reference [18] presented a collaborative optimization framework for mobile ocean MGs, applying a collective decision-making algorithm to minimize operation costs while maximizing system resilience. Reference [19] addressed coordinated operation under both normal and emergency conditions through a two-stage stochastic multi-objective planning model, incorporating a resilience index to quantify system recovery capability.

Table I summarizes the relevant features of the past studies and this paper and identifies important technical issues limiting the coordination efficiency of DN and MG. First, although distributed algorithms offer strong privacy protection for individual participants, their reliance on iterative solution processes results in slow convergence, limiting their suitability for real-time dispatch. Similarly, deep reinforcement learning approaches demand extensive historical data, which restrict their applicability in data-sparse or isolated environments. Second, and more crucially pertaining to the core of flexible coordination, the existing research work lacks the absence of a precise and computationally tractable model for quantifying and evaluating regulation potential of MG at the point of common coupling (PCC), making it challenging to meet the fine-grained coordination requirements of DN.

TABLE I
COMPARISON OF RELEVANT FEATURES OF PAST STUDIES AND THIS PAPER

Ref.	Objective				Architecture		Interaction		Pricing			PCC adjustability
	Economy	Environment	Robustness	Resilience	Distributed	Centralized	Iterative	Non-iterative	Multi-step time of use	Two-step peak-valley	Fixed	
[9]	✓	×	×	×	×	✓	×	✓	×	✓	✓	×
[10]	✓	✓	✓	×	×	✓	✓	×	×	×	✓	×
[11]	✓	×	×	×	✓	×	✓	×	✓	×	×	×
[12]	✓	×	×	×	✓	×	✓	×	✓	×	×	×
[13]	✓	×	×	×	✓	×	✓	×	×	×	✓	×
[14]	✓	×	×	✓	×	✓	✓	×	×	×	×	×
[15]	✓	×	✓	×	×	✓	×	✓	✓	×	×	×
[16]	✓	×	✓	×	×	✓	✓	×	✓	×	×	×
[17]	✓	×	×	✓	×	✓	×	✓	✓	×	×	×
[18]	✓	×	×	✓	×	✓	×	✓	×	×	✓	×
[19]	✓	×	✓	✓	×	✓	×	✓	×	✓	×	×
This paper	✓	×	×	×	✓	×	×	✓	✓	×	×	✓

Note: ✓ and × indicate having or not having the corresponding characteristics, respectively.

To deal with these aforementioned gaps, this paper presents a coordinated dispatch framework of DN and MG (termed as the proposed CD framework hereafter) with a cross-layer flexibility mechanism to support both flexible and economical operation of DN and MG. We introduce the concept of the MG flexible operation region (MGFOR) to quantify the adjustable capacity of MG with massive FRs, e.g., photovoltaic (PV), ESS, and FL. While several studies have explored region-based coordination of DN and MG, such as the non-iterative equivalent projection approach [20] and the fast approximation algorithms for high-dimensional problems [21], most have focused solely on technical feasibility or computational efficiency, neglecting economically-aware flexibility provision and active voltage support capabilities from MGs. In contrast, the MGFOR model captures the feasible active/reactive power regulation range at the PCC by solving a sequence of optimal power flow (OPF) problems under varying aggregated regulation cost (ARC), with a convex-hull fitting approach applied to generate observable flexible operation region space. Building on this model, the proposed CD framework is developed. The DN layer minimizes the sum of operation costs and voltage deviation penalty at the PCC by utilizing MGs for active voltage support. The MG layer focuses on minimizing local operation costs. In the end, the principal contributions of this paper are summarized as follows.

1) An MGFOR model is constructed to precisely characterize the regulation capability of MG under large-scale FR integration, with the influence of ARC constraints on MGFOR explicitly being analyzed.

2) The MGFOR is visually and mathematically characterized via a convex-hull fitting approach and serves as the foundation of the proposed CD framework. In this framework, MGFOR acts as the information interaction interface, facilitating efficient coordination while strictly preserving data privacy.

3) Simulation on a modified IEEE 33-node test system shows that the number of ARC tiers directly impacts the coordination performance and underscores the necessity of reactive power support of distributed PV units for maintaining voltage quality during peak-demand periods in the evening.

The rest of the paper is structured as follows. Section II presents the proposed CD framework. Section III details the solution approach. Section IV discusses the simulation results. Section V concludes the paper.

II. Proposed CD Framework

A. Core Concept

MGFOR is defined as the set of feasible operation states of MG that comply with the power balance constraints, the operation limits of integrated FRs, and the ARC constraints over the dispatch cycle. This definition accounts for the real-time response capabilities of multiple FR types within MG. The operation state of MG is characterized by its active and reactive power demands at the PCC, resulting in a compact representation of the MGFOR model as:

$$\mathbb{Z}_t^{\mathrm{MGFOR}} = \Big\{ \boldsymbol{x} = \left[P_t^{\mathrm{DM}}, Q_t^{\mathrm{DM}} \right] \Big| \boldsymbol{g}\left(\boldsymbol{x},\boldsymbol{y}\right) = \boldsymbol{0}, \boldsymbol{f}\left(\boldsymbol{x},\boldsymbol{y}\right) \le \boldsymbol{0}, c\left(\boldsymbol{x},\boldsymbol{y}\right) \le \lambda, \boldsymbol{y} \in \mathbb{R}^n, t \in T \Big\} \tag{1}$$

where $\boldsymbol{x}$ is the target observation vector comprising the active power demand P_t^{DM} and reactive power demand Q_t^{DM} at the PCC at time t; $\boldsymbol{y}$ is the internal vector containing all other variables within MG, such as distributed generation outputs and controllable loads; λ is the parameter representing the maximum allowable ARC; $\boldsymbol{g}(\cdot)=\boldsymbol{0}$, $\boldsymbol{f}(\cdot)=\boldsymbol{0}$, and $c(\cdot)\le\lambda$ are the constraints denoting the power balance constraint, the safe operation constraint for FRs, and the ARC constraint, respectively; $\mathbb{R}^n$ denotes the n-dimensional vector space; and T is the set of time in the dispatch cycle.

The introduction of the ARC constraints into the MGFOR model is motivated by both practical operation demands and model generality considerations. On the one hand, the ARC constraints provide MG with a clear and intuitive cost ceiling, which aligns with the requirement of DSO to request flexibility services within a budget, thereby ensuring that MG operates within an economically feasible range. On the other hand, since the composition of FRs varies among different types of MGs, the ARC constraints serve as a universal form of constraint that can effectively accommodate diverse MG configurations.

Additionally, the active and reactive power demands at the PCC are selected as the key decision variables in the MGFOR model for the following reasons.

1) They represent the most direct form of interaction between DN and MG, aligning with the operation intuition of grid operators.

2) The power demand range at the PCC encapsulates the internal flexibility capacity of MG, enabling effective data privacy protection while meeting the information security requirements arising from DN and MG operated by separate entities.

3) The resulting two-dimensional observation vectors facilitate intuitive visualization and convenient monitoring of the MGFOR model.

B. Construction of MGFOR

Owing to the variations in the types and capacities of integrated FRs, MGs demonstrate distinct operation characteristics. Based on their functional attributes, FRs can be classified into three types.

1) Generation-side FRs: system fluctuations are mitigated through adjustments in the active and reactive outputs of grid-connected units. Conventional sources, e.g., gas and coal-fired units, possess bidirectional active power regulation capabilities. In contrast, distributed generation units, e.g., PVs and wind turbines (WTs), are constrained by environmental conditions, rendering active power largely uncontrollable; however, reactive power regulation is achievable via inverter control.

2) Storage-side FRs: ESS enables spatiotemporal redistribution of power through energy shifting and two-way regulation. Lithium-ion battery systems are typically employed for this purpose.

3) Demand-side FRs: dynamic demand is facilitated by modulating or redispatching the consumption patterns of adjustable loads, e.g., heating, ventilation, and air conditioning (HVAC), and electric water heaters, and shiftable loads, e.g., electric vehicle (EV) chargers and selected household appliances.

To demonstrate the synergistic operation of these FR types, an MG consisting PV, ESS, and FL (termed as PV-ESS-FL MG hereafter) is modeled as a representative case in this paper.

1) Modeling of PV-ESS-FL MG

In this paper, an MGFOR model is developed incorporating distributed PV, shared ESS, and temperature-controlled FL. The model is constrained by the following considerations.

1) Power balance constraints

In a typical low-voltage MG (LV-MG), short transmission distances result in line resistance significantly exceeding reactance, thereby minimizing the influence of reactive power on voltage profiles. Under such conditions, real-time active power balancing becomes the primary operation objective. Consequently, the MG power flow equations can be simplified to active power balance constraints as:

$$P_t^{\mathrm{DM}_m}+\sum_{g\in I_{\mathrm{MG}_m}^{\mathrm{PV}}}P_{g,t}^{\mathrm{PV}}+\sum_{f\in I_{\mathrm{MG}_m}^{\mathrm{ESS}}}\left(P_{f,t}^{\mathrm{dis}}-P_{f,t}^{\mathrm{ch}}\right)=\sum_{h\in I_{\mathrm{MG}_m}^{\mathrm{HVAC}}}P_{h,t}^{\mathrm{HVAC}}+P_{L,t} \tag{2a}$$

$$Q_t^{\mathrm{DM}_m}+\sum_{g\in I_{\mathrm{MG}_m}^{\mathrm{PV}}}Q_{g,t}^{\mathrm{PV}}=\sum_{h\in I_{\mathrm{MG}_m}^{\mathrm{HVAC}}}Q_{h,t}^{\mathrm{HVAC}}+Q_{L,t} \tag{2b}$$

where $P_t^{\mathrm{DM}_m}$ and $Q_t^{\mathrm{DM}_m}$ are the active and reactive power exchanged between MG m and DN at time t, respectively; $P_{g,t}^{\mathrm{PV}}$ and $Q_{g,t}^{\mathrm{PV}}$ are the active output and reactive compensation of distributed PV unit g at time t, respectively; $P_{f,t}^{\mathrm{ch}}$ and $P_{f,t}^{\mathrm{dis}}$ are the charging and discharging power of ESS f at time t, respectively; $P_{h,t}^{\mathrm{HVAC}}$ and $Q_{h,t}^{\mathrm{HVAC}}$ are the active and reactive power demands of HVAC unit h at time t, respectively; $I_{\mathrm{MG}_m}^{\mathrm{PV}}$, $I_{\mathrm{MG}_m}^{\mathrm{ESS}}$, and $I_{\mathrm{MG}_m}^{\mathrm{HVAC}}$ are the index sets of distributed PV units, ESSs, and HVAC units in MG m, respectively; and $P_{L,t}$ and $Q_{L,t}$ are the active and reactive power demands of the local load at time t, respectively.

2) Distributed PV operation constraints

Assuming the full use of the distributed PV output within MG and considering its reactive power support capability, the secure operation of each distributed PV unit g is required to satisfy:

$$-P_{g,t}^{\mathrm{PV}}\tan\varphi_{g,\max}\le Q_{g,t}^{\mathrm{PV}}\le P_{g,t}^{\mathrm{PV}}\tan\varphi_{g,\max} \tag{3a}$$

$$\left(P_{g,t}^{\mathrm{PV}}\right)^2+\left(Q_{g,t}^{\mathrm{PV}}\right)^2\le\left(S_g^{\mathrm{PV}}\right)^2 \tag{3b}$$

where $\varphi_{g,\max}$ is the maximum permissible power factor angle of the distributed PV unit g; and S_g^{PV} is the rated apparent power capacity of the distributed PV unit g.

3) ESS operation constraints

The state of charge (SOC) of an ESS is governed by its charging and discharging dynamics and rated capacity, which must comply with operation exclusivity, i.e., charging and discharging cannot occur simultaneously. The secure operation of ESS f at time t is subjected to:

$$\begin{cases}0\le P_{f,t}^{\mathrm{ch}}\le u_{f,t}^{\mathrm{ch}}P_{f,\max}^{\mathrm{ch}}\\0\le P_{f,t}^{\mathrm{dis}}\le u_{f,t}^{\mathrm{dis}}P_{f,\max}^{\mathrm{dis}}\end{cases} \tag{4a}$$

$$u_{f,t}^{\mathrm{ch}}+u_{f,t}^{\mathrm{dis}}\le 1 \tag{4b}$$

$$E_{f,t+1}=E_{f,t}+P_{f,t}^{\mathrm{ch}}\eta_{f,\mathrm{ch}}\Delta t-\frac{P_{f,t}^{\mathrm{dis}}\Delta t}{\eta_{f,\mathrm{dis}}} \tag{4c}$$

$$E_{f,\min}\le E_{f,t}\le E_{f,\max} \tag{4d}$$

where $u_{f,t}^{\mathrm{ch}}$ and $u_{f,t}^{\mathrm{dis}}$ are the binary variables indicating the charging and discharging states of ESS f at time t, respectively; $E_{f,t}$ is the power of ESS f at the beginning of time t; $\eta_{f,\mathrm{ch}}$ and $\eta_{f,\mathrm{dis}}$ are the charging and discharging efficiencies of ESS f, respectively; $P_{f,\max}^{\mathrm{ch}}$ and $P_{f,\max}^{\mathrm{dis}}$ are the maximum charging and discharging power of ESS f, respectively; and $E_{f,\max}$ and $E_{f,\min}$ are the upper and lower limits of the capacity of ESS f, respectively.

4) HVAC operation constraints

HVAC, as a temperature-controlled FL, can be dynamically adjusted while maintaining user thermal comfort. Considering the thermal inertia of the building, its safe operation must be ensured, which is mathematically represented as:

$$\underline{P}_h^{\mathrm{HVAC}}\le P_{h,t}^{\mathrm{HVAC}}\le\overline{P}_h^{\mathrm{HVAC}} \tag{5a}$$

$$Q_{h,t}^{\mathrm{HVAC}}=\eta_h P_{h,t}^{\mathrm{HVAC}} \tag{5b}$$

$$\underline{F}_h\le F_{h,t}^{\mathrm{in}}\le\overline{F}_h \tag{5c}$$

$$F_{h,t}^{\mathrm{in}}=F_{h,t-1}^{\mathrm{in}}+\alpha_h\left(F_t^{\mathrm{out}}-F_{h,t-1}^{\mathrm{in}}\right)+\Delta t\beta_h P_{h,t}^{\mathrm{HVAC}} \tag{5d}$$

where $\underline{P}_h^{\mathrm{HVAC}}$ and $\overline{P}_h^{\mathrm{HVAC}}$ are the lower and upper limits of the active power when HVAC unit h is in operation, respectively; η_h is a constant reflecting the impedance ratio of HVAC unit h; $\underline{F}_h$ and $\overline{F}_h$ are the lower and upper limits of the permissible indoor temperature of HVAC unit h, respectively; $F_{h,t}^{\mathrm{in}}$ is the indoor temperature of HVAC unit h at the end of time t; F_t^{out} is the outdoor temperature at time t; $\alpha_h\in(0,1)$ and β_h signify the thermal characteristics of the building and the environment, respectively, with the positive and negative values of β_h corresponding to heating and cooling modes of HVAC unit h; and Δt is the time interval.

5) ARC constraints

The ARC constraints, accounting for the cooperative responsiveness of various FRs within an MG, enable the DSO to quantify power regulation capabilities without disclosing sensitive MG information.

$$\lambda\ge C_t^{\mathrm{RE}}=C_t^{\mathrm{HVAC}}+C_t^{\mathrm{ESS}}+C_t^{\mathrm{PV}}=\sum_{h\in I_{\mathrm{MG}_m}^{\mathrm{HVAC}}}C_{h,t}^{\mathrm{HVAC}}+\sum_{f\in I_{\mathrm{MG}_m}^{\mathrm{ESS}}}C_{f,t}^{\mathrm{ESS}}+\sum_{g\in I_{\mathrm{MG}_m}^{\mathrm{PV}}}C_{g,t}^{\mathrm{PV}} \tag{6a}$$

$$\lambda_l=\frac{C_{\max}^{\mathrm{RE}}-C_{\min}^{\mathrm{RE}}}{L}l+C_{\min}^{\mathrm{RE}}\quad l=1,2,\dots,L \tag{6b}$$

$$C_{h,t}^{\mathrm{HVAC}}=\lambda_t^{\mathrm{HVAC}}\left|\Delta P_{h,t}\right|=\lambda_t^{\mathrm{HVAC}}\left|P_{h,t}^{\mathrm{HVAC}}-P_{h,b,t}^{\mathrm{HVAC}}\right| \tag{6c}$$

$$C_{f,t}^{\mathrm{ESS}}=\lambda_{f,t}^{\mathrm{dis}}P_{f,t}^{\mathrm{dis}}-\lambda_{f,t}^{\mathrm{ch}}P_{f,t}^{\mathrm{ch}} \tag{6d}$$

$$\begin{cases}\lambda_{f,t}^{\mathrm{ch}}=C_{\mathrm{MG},t}^{\mathrm{buy}}/\eta_{f,\mathrm{ch}}+\lambda_{\mathrm{op}}\\\lambda_{f,t}^{\mathrm{dis}}=C_{\mathrm{MG},t}^{\mathrm{buy}}\eta_{f,\mathrm{dis}}-\lambda_{\mathrm{op}}\end{cases} \tag{6e}$$

$$C_{g,t}^{\mathrm{PV}}=\begin{cases}\lambda^{\mathrm{RPC}}Q_{g,t}^{\mathrm{PV}} & Q_{g,t}^{\mathrm{PV}}\ge 0\\0 & Q_{g,t}^{\mathrm{PV}}<0\end{cases} \tag{6f}$$

where $C_{h,t}^{\mathrm{HVAC}}$, $C_{f,t}^{\mathrm{ESS}}$, and $C_{g,t}^{\mathrm{PV}}$ are the adjustment costs of HVAC unit h, ESS f, and distributed PV unit g at time t, respectively; L is the total number of ARC tiers l; $C_{\max}^{\mathrm{RE}}$ and $C_{\min}^{\mathrm{RE}}$ are the upper and lower bounds of ARC corresponding to the maximum cost paid by the MG operator to fully use the FR service capacity and the minimum cost for the FRs to participate in regulation, respectively; $\lambda_t^{\mathrm{HVAC}}$ is the subsidy factor based on the power purchase tariff at time t; $\Delta P_{h,t}$ is the regulated power of HVAC unit h participating in DR at time t, and HVAC unit h is allowed to reduce power during peak-demand periods ($\Delta P_{h,t} \geq 0$) and increase power during valley-demand periods ($\Delta P_{h,t} \leq 0$); $P_{h,b,t}^{\mathrm{HVAC}}$ is the baseline power of HVAC unit h at time t; $\lambda_{f,t}^{\mathrm{ch}}$ and $\lambda_{f,t}^{\mathrm{dis}}$ are the charging cost coefficient and discharging yield coefficient of ESS f at time t, respectively; $C_{\mathrm{MG},t}^{\mathrm{buy}}$ is the power purchase tariff of MG at time t; λ_{op} is the action cost factor; and λ^{RPC} is a fixed subsidy factor.

An equally spaced discretization of λ is determined based on the upper and lower bounds of ARC, enabling cooperative utilization of the cost-tiered regulation capacity of MG by DN. For the three types of FRs, the specific adjustment cost is calculated as follows.

1) Based on electricity price discounts and capacity reimbursement, the incentive subsidies for customer-side HVAC participate in DR.

2) The user-side ESS of the MG benefits from using the peak-to-valley price difference by dispatching charging during valley-demand periods and discharging during peak-demand periods.

3) Given the bidirectional reactive power regulation capability of distributed PV, subsidies are assumed to be granted only when it operates in inductive mode.

In summary, MG dynamically reconfigures its MGFOR in response to changes at ARC tier l to meet DN regulation requirements.

2) Linearized Characterization of MGFOR Based on Convex-hull Fitting

According to Section II-B-1), the MGFOR boundary at ARC tier l is represented by a set of discrete boundary points P_{MGFOR}^{l} as shown in (7). $\mathcal{P}_{\mathrm{MGFOR}}^{l}$ consists of R discrete boundary points, each represented by an active-reactive power pair $[P_{t,l,r}^{\mathrm{DM}_m}, Q_{t,l,r}^{\mathrm{DM}_m}]$, and $r=1,2,\ldots,R$ is the index of the discrete points.

$$\mathcal{P}_{\mathrm{MGFOR}}^{l} = \left\{ \left[P_{t,l,1}^{\mathrm{DM}_m}, Q_{t,l,1}^{\mathrm{DM}_m} \right], \ldots, \left[P_{t,l,R}^{\mathrm{DM}_m}, Q_{t,l,R}^{\mathrm{DM}_m} \right] \right\} \tag{7}$$

By using the convex-hull fitting approach [22], the set of ordered convex-hull vertices $vert\left(\mathbb{Z}_{t,l}^{\mathrm{MGFOR}}\right)$ is extracted from P_{MGFOR}^{l} as shown in (8). Consequently, MGFOR is transformed into a segmented linear constraint as shown in (9).

$$vert\left(\mathbb{Z}_{t,l}^{\mathrm{MGFOR}}\right) = \left\{ \left[P_{t,l,[1]}^{\mathrm{DM}_m}, Q_{t,l,[1]}^{\mathrm{DM}_m} \right], \ldots, \left[P_{t,l,[D]}^{\mathrm{DM}_m}, Q_{t,l,[D]}^{\mathrm{DM}_m} \right] \right\} \tag{8}$$

$$\begin{cases} P_{t,l}^{\mathrm{DM}_m} = \sum\limits_{d=1}^{D} \tau_{l,d} P_{t,l,[d]}^{\mathrm{DM}_m} & \tau_{l,d} \geq 0 \\ Q_{t,l}^{\mathrm{DM}_m} = \sum\limits_{d=1}^{D} \tau_{l,d} Q_{t,l,[d]}^{\mathrm{DM}_m} & \sum\limits_{d=1}^{D} \tau_{l,d} = 1 \end{cases} \tag{9}$$

where $P_{t,l,[d]}^{\mathrm{DM}_m}$ and $Q_{t,l,[d]}^{\mathrm{DM}_m}$ form the d^{th} convex-hull vertex; $\tau_{l,d}$ is the corresponding segmentation factor; and D is the number of convex-hull vertices.

Based on (8), after redundant boundary points are eliminated, a linearized representation of MGFOR is achieved through (9), which reduces model complexity, enhances solution efficiency, and ensures model convexity while strictly maintaining solution feasibility.

The solution approach for $\mathcal{P}_{\mathrm{MGFOR}}^{l}$ is discussed in detail in Section III, with this subsection assuming that $\mathcal{P}_{\mathrm{MGFOR}}^{l}$ focuses on the MGFOR characterization.

C. Co-optimization of DN and MG Based on MGFOR

1) Coordinated Optimization Strategy of DN and MG

A cross-tier flexibility co-allocation strategy is designed for co-optimization of DN and MG, inspired by the approach in [23], as shown in Supplementary Material A Fig. SA1.

The MGFOR is first constructed by aggregating the FRs of MG and then linearized using the convex-hull fitting approach. The MG dispatch center uploads MGFOR as boundary interaction data to the DN dispatch center, which determines the interaction power based on its objectives. Finally, MG performs local flexibility decomposition to minimize operation costs and optimize the allocation of internal FRs.

2) DN Layer Model

The DN dispatch aims to minimize operation costs while ensuring that MG provides voltage support, focusing on minimizing the voltage deviation at the PCC from the reference voltage [24].

$$\begin{aligned} \min C_t^{\mathrm{DN}} = & C_{\mathrm{buy},t}^{\mathrm{DN}} P_{\mathrm{sub},t}^{\mathrm{DN}} - C_{\mathrm{buy},t}^{\mathrm{MG}} \sum_{i \in N} P_{i,t}^{\mathrm{IPF}_m} + \\ & \sum_{i \in N} \left(C_{\mathrm{ESS},t}^{\mathrm{dis}} P_{i,t}^{\mathrm{dis}} - C_{\mathrm{ESS},t}^{\mathrm{ch}} P_{i,t}^{\mathrm{ch}} \right) + \lambda^{\mathrm{shed}} \sum_{i \in N} \Delta P_{i,t}^{\mathrm{load}} + \\ & \sum_{m \in M} \mu_t^{\mathrm{MG}_m} \left| v_{0,t}^{\mathrm{MG}_m} - v_{0,\mathrm{ref},t}^{\mathrm{MG}_m} \right| \end{aligned} \tag{10}$$

where $C_{\mathrm{buy},t}^{\mathrm{DN}}$ is the electricity purchase price for DN at time t; $P_{\mathrm{sub},t}^{\mathrm{DN}}$ is the active power acquired by the root node of DN from the upper-level grid at time t; $P_{i,t}^{\mathrm{IPF}_m}$ is the active power transferred from node i of DN to the connected MG m at time t; $P_{i,t}^{\mathrm{ch}}$ and $P_{i,t}^{\mathrm{dis}}$ are the charging and discharging power of the ESS at node i of DN at time t, respectively; $C_{\mathrm{ESS},t}^{\mathrm{ch}}$ and $C_{\mathrm{ESS},t}^{\mathrm{dis}}$ are the charging cost and discharging revenue of the ESS of DN at time t, respectively; λ^{shed} is the lost load penalty factor; $\Delta P_{i,t}^{\mathrm{load}}$ is the load curtailment at node i of DN; $v_{0,t}^{\mathrm{MG}_m}$ and $v_{0,\mathrm{ref},t}^{\mathrm{MG}_m}$ are the actual and reference voltages at the PCC of MG m at time t, respectively; and $\mu_t^{\mathrm{MG}_m}$ is the voltage deviation weight factor at the PCC of MG m. $\mu_t^{\mathrm{MG}_m}$ quantifies the priority assigned to the voltage deviation at the PCC within the optimization objective of DN. An appropriate value for this coefficient ensures effective voltage support from MG while maintaining the economic operation of DN. Additionally, $C_{\mathrm{ESS},t}^{\mathrm{ch}}$ and $C_{\mathrm{ESS},t}^{\mathrm{dis}}$ are determined using the same approach described in (6e) and are not reiterated here.

1) Trend balancing constraints

DN typically operates under a radial topology, and its current flow is modeled using the branch-current model in [25] as:

$$P_{i,t} = \sum_{j \in F(i)} P_{ij,t} - \sum_{k \in T(i)} \left(P_{ki,t} - l_{ki,t} r_{ki} \right) \tag{11a}$$

$$Q_{i,t} = \sum_{j \in F(i)} Q_{ij,t} - \sum_{k \in T(i)} \left(Q_{ki,t} - l_{ki,t} x_{ki} \right) \tag{11b}$$

$$V_{j,t} = V_{i,t} - 2\left(P_{ij,t} r_{ij} + Q_{ij,t} x_{ij} \right) + l_{ij,t}\left(r_{ij}^2 + x_{ij}^2 \right) \tag{11c}$$

$$\left\|\begin{matrix} 2P_{ij,t} \\ 2Q_{ij,t} \\ l_{ij,t}-V_{i,t} \end{matrix}\right\|_2 \le l_{ij,t}+V_{i,t} \tag{11d}$$

$$P_{ij,t}^2+Q_{ij,t}^2 \le S_{ij}^2 \tag{11e}$$

$$V_{i,\min} \le V_{i,t} \le V_{i,\max} \tag{11f}$$

where $P_{i,t}$ and $Q_{i,t}$ are the active and reactive power injected at node i of DN at time t, respectively; $F(i)$ and $T(i)$ are the sets referring to the child and parent nodes connected to node i, respectively; $P_{ki,t}$ and $Q_{ki,t}$ are the active and reactive power flows through branch ki at time t, respectively; $P_{ij,t}$ and $Q_{ij,t}$ are the active and reactive power flows through branch ij at time t, respectively; S_{ij} is the rated power capacity of branch ij; l_{ki} and l_{ij} are the squared current magnitudes of branches ki and ij, respectively; r_{ki} and x_{ki} are the resistance and reactance of branch ki, respectively; r_{ij} and x_{ij} are the resistance and reactance of branch ij, respectively; $V_{i,\min}$ and $V_{i,\max}$ are the minimum and the maximum voltage magnitudes at node i, respectively; and $V_{i,t}$ is the squared voltage magnitude at node i at time t.

In constraints (11a) and (11b), $P_{i,t}$ and $Q_{i,t}$ are calculated by the generation output, load demand, and interconnection power at node i. The line voltage drop constraint is represented by constraint (11c). Constraint (11d) uses second-order cone relaxation to replace the quadratic equality $l_{ij,t}V_{i,t}=P_{ij,t}^2+Q_{ij,t}^2$, improving solution efficiency while retaining accuracy. Constraints (11e) and (11f) enforce limits on nodal voltage magnitude and line transmission capacity, respectively, ensuring the secure and stable operation of DN.

2) Operation constraints of PV power station with centralized ESS

The DN-side PV station and centralized ESS adhere to the same operation constraints as the distributed PV and ESS outlined in Section II-B, with the only difference being in the operation parameters.

3) Boundary coupling constraints of DN and MG

The DN is connected to MG via a contact transformer, with the boundary coupling represented by the consistency of active and reactive power on both sides of the tie line. Based on (9), the boundary coupling constraints derived from the convex hull are expressed as:

$$P_{i,t}^{\mathrm{IPF}_m}=\sum_{l=1}^{L} s_l P_{t,l}^{\mathrm{DM}_m} \tag{12a}$$

$$Q_{i,t}^{\mathrm{IPF}_m}=\sum_{l=1}^{L} s_l Q_{t,l}^{\mathrm{DM}_m} \tag{12b}$$

$$\sum_{l=1}^{L} s_l=1 \tag{12c}$$

where s_l is the 0-1 variable corresponding to ARC tier l. When $s_l=1$, it indicates that DN selects MGFOR under ARC tier l. The mutual exclusivity in constraint (12c) ensures the uniqueness of the tier selection.

3) MG Layer Model

The MG dispatch aims to minimize its local operation cost based on the boundary interaction power determined by the DN dispatch center.

$$\min C_t^{\mathrm{MG}_m}=C_{\mathrm{MG},t}^{\mathrm{buy}}P_t^{\mathrm{DM}_m}+C_{\mathrm{MG},t}^{\mathrm{HVAC}}+C_{\mathrm{MG},t}^{\mathrm{ESS}}+C_{\mathrm{MG},t}^{\mathrm{PV}} \tag{13}$$

Because MG has met the cooperative demand of DN, it focuses on economically optimizing the decomposition of local flexibility demand to determine the dispatch strategy for each FR.

The MG layer model must satisfy both operation feasibility and equipment security requirements. The constraints include power balance constraints and safe operation constraints of FRs. The constraints that are consistent with the MGFOR model are employed, ensuring the convergence of the co-optimization process of DN and MG.

III. Solution Approach

A. Acquisition of Original Set of Boundary Points

The MGFOR considers the active and reactive power at the PCC as target observation variables. Inspired by the approach in [26], an OPF model is constructed to minimize $P_{t,l}^{\mathrm{DM}_m}$ and $Q_{t,l}^{\mathrm{DM}_m}$ by iteratively adjusting parameters, thereby obtaining the set of boundary points $\mathcal{P}_{\mathrm{MGFOR}}^{l}$.

$$\min H(\alpha,\beta)=\alpha P_{t,l}^{\mathrm{DM}_m}+\beta Q_{t,l}^{\mathrm{DM}_m} \tag{14}$$

where α and β are the adjustable parameters. A radial iterative search rule is applied to track each boundary point sequentially, with specific values for α and β defined as:

$$\begin{cases} \alpha=\cos(\theta_0+\mu\Delta\theta) \\ \beta=\sin(\theta_0+\mu\Delta\theta) \end{cases} \quad \mu=0,1,\ldots,K,\ K\Delta\theta=2\pi \tag{15}$$

where θ_0 is the initial search angle; $\Delta\theta$ is the search angle step; μ is the iteration number; and K is the total number of search iterations.

B. Linearized Equivalent Substitution

Constraints (6f), (12a), and (12b), as well as the objective function (10), introduce non-convexities due to the products of binary and continuous variables and the presence of absolute value terms, which can be reformulated equivalently.

1) The big-M approach is employed to linearize constraint (6f).

$$C_{g,t}^{\mathrm{PV}} \ge 0 \tag{16a}$$

$$C_{g,t}^{\mathrm{PV}} \ge M b_{g,t} \tag{16b}$$

$$C_{g,t}^{\mathrm{PV}} \le -M b_{g,t} \tag{16c}$$

$$C_{g,t}^{\mathrm{PV}} \le \lambda^{\mathrm{RPC}} Q_{g,t}^{\mathrm{PV}}-M\left(1-b_{g,t}\right) \tag{16d}$$

$$C_{g,t}^{\mathrm{PV}} \ge \lambda^{\mathrm{RPC}} Q_{g,t}^{\mathrm{PV}} \tag{16e}$$

where $b_{g,t}$ is a binary variable indicating the operation mode of distributed PV unit g at time t; and M is a sufficiently small constant.

2) The constraints (12a) and (12b) are non-convex due to the bilinear terms $s_l P_{t,l}^{\mathrm{DM}_m}$ and $s_l Q_{t,l}^{\mathrm{DM}_m}$, respectively. To preserve model tractability, we introduce an auxiliary variable $z_{l,d}$ and apply the McCormick envelope approach for exact linearization.

$$z_{l,d}=s_l\tau_{l,d} \tag{17a}$$

$$z_{l,d} \le \tau_{l,d} \tag{17b}$$

$$z_{l,d} \le s_l \tag{17c}$$

$$z_{l,d} \ge \tau_{l,d} + s_l - 1 \tag{17d}$$

$$z_{l,d} \ge 0 \tag{17e}$$

Thus, constraints (12a) and (12b) can be reformulated as:

$$P_{i,t}^{\mathrm{IPF}_m} = \sum_{l=1}^{L}\sum_{d=1}^{D} z_{l,d} P_{t,l,[d]}^{\mathrm{DM}_m} \tag{18a}$$

$$Q_{i,t}^{\mathrm{IPF}_m} = \sum_{l=1}^{L}\sum_{d=1}^{D} z_{l,d} Q_{t,l,[d]}^{\mathrm{DM}_m} \tag{18b}$$

3) The objective function (10) can be rephrased as:

$$\min C_t^{\mathrm{DN}} = C_{\mathrm{buy},t}^{\mathrm{DN}} P_{\mathrm{sub},t}^{\mathrm{DN}} - C_{\mathrm{buy},t}^{\mathrm{MG}} \sum_{i \in N} P_{i,t}^{\mathrm{IPF}_m} + \sum_{i \in N}\left(C_{\mathrm{ESS},t}^{\mathrm{dis}} P_{i,t}^{\mathrm{dis}} - C_{\mathrm{ESS},t}^{\mathrm{ch}} P_{i,t}^{\mathrm{ch}}\right) + \lambda^{\mathrm{shed}} \sum_{i \in N} \Delta P_{i,t}^{\mathrm{load}} + \sum_{m \in M} \mu_t^{\mathrm{MG}_m} V_{t,\mathrm{dev}}^{\mathrm{MG}_m} \tag{19}$$

where $V_{t,\mathrm{dev}}^{\mathrm{MG}_m}$ is an auxiliary variable in place of the absolute value term.

C. Discussion on Accuracy and Validity of Linearization

To ensure the tractability of the proposed CD framework, several linearization techniques are employed.

1) Convex-hull Approximation for MGFOR

The accuracy of describing MGFOR with a convex hull depends on $\Delta\theta$ and K. With the increase of K, more vertices can be obtained to improve the accuracy of the convex-hull approximation, at the expense of increased computational burden. Therefore, it is necessary to select an appropriate search step size to balance computational efficiency and solution accuracy. In the case study in Section IV, it is demonstrated that with $\Delta\theta = 5°$ and $K = 72$, the approximation error becomes negligible.

2) Big-M Linearization for Constraint (6f)

The value of M must be sufficiently small to ensure that no feasible solutions are cut off, yet not excessively small to avoid introducing numerical instability. Analysis of constraints (16a)-(16e) shows that only $M < -\max C_{g,t}^{\mathrm{PV}}$ ensures that the linearization is exact without sacrificing feasibility.

3) McCormick Linearization for Constraints (12a) and (12b)

The McCormick envelope approach provides an exact McCormick linearization for products of binary and continuous variables. By implementing this approach, the DSO can freely select from MGFORs across different ARC tiers, ensuring the model feasibility regardless of whether MG imports or exports power from or to DN.

4) Linearization of Absolute Value in Objective Function (10)

The absolute value of voltage deviation in the objective function (10) is reformulated using the auxiliary variable $V_{t,\mathrm{dev}}^{\mathrm{MG}_m}$ and three linear inequality constraints as follows, which constitutes an exact reformulation without approximation error when the objective function is minimized.

$$v_{0,t}^{\mathrm{MG}_m} - v_{0,\mathrm{ref},t}^{\mathrm{MG}_m} \le V_{t,\mathrm{dev}}^{\mathrm{MG}_m} \tag{20a}$$

$$v_{0,t}^{\mathrm{MG}_m} - v_{0,\mathrm{ref},t}^{\mathrm{MG}_m} \ge -V_{t,\mathrm{dev}}^{\mathrm{MG}_m} \tag{20b}$$

$$V_{t,\mathrm{dev}}^{\mathrm{MG}_m} \ge 0 \tag{20c}$$

By integrating the above conditions, the co-optimization of DN and MG is achieved through the solution of the convex mixed-integer quadratic-constrained programming (MIQCP) problem. Furthermore, given the convexity of the true feasible region, MGFOR, constructed strictly from P_{MGFOR}^{l}, inherently constitutes a conservative approximation. This ensures that no infeasible operation points are introduced. Consequently, any operation point selected by the DSO within MGFOR is guaranteed to be realizable by MG through the dispatch of its internal FRs.

IV. Case Study

An IEEE 33-node test system [27], as shown in Fig. 1, is constructed with a DN operated at 12.66 kV. The DN exhibits peak active and reactive loads of 4584 kW and 2272 kvar, respectively, with a root node voltage of 1.05 p.u.. Three PV plants and corresponding centralized ESSs are integrated into the system.

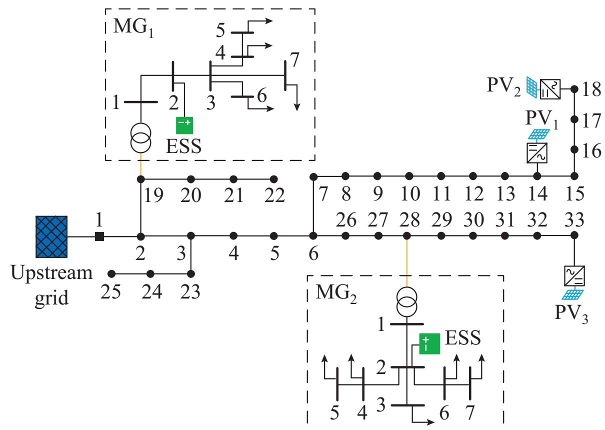

Fig. 1. Topology of IEEE 33-node test system.

Residential MG$_1$ and industrial park MG$_2$ are connected to nodes 19 and 28, respectively, via contact transformers rated at 12.66 kV/380 V. MG$_1$ consists of four residential buildings (RB$_1$-RB$_4$), each equipped with distributed PV units and centralized HVAC units, along with a community-level ESS. MG$_2$ includes two rooftop distributed PV units, two commercial buildings (CB$_1$ and CB$_2$) with HVAC systems, and one ESS.

The remaining parameters are specified as follows. The ESS capacity is constrained between 10% and 90% of its rated value, with the initial state set to be the upper limit of its capacity, and $\lambda_{\mathrm{op}} = 0.014$ \$/kWh. The indoor temperature comfort range is maintained between 23 °C and 26.5 °C; $F_{h,0}^{\mathrm{in}} = 24.5$; $\lambda^{\mathrm{RPC}} = 0.058$ \$/kvar; $\lambda^{\mathrm{shed}} = 2.5$ \$/kW; the permissible upper and lower limits of the system voltage are 1.1 p.u. and 0.9 p.u., respectively; $L = 8$; and $\Delta t = 1$ hour. Furthermore, the case studies in this paper also investigate the extreme high-temperature condition and are supported by complete datasets for both scenarios, available via an online supplement [28]. The formulated MIQCP problem is solved using GUROBI and CPLEX solvers on a computer platform equipped with a 2.2 GHz Intel Core-i9 processor and 16 GB RAM.

A. Computational Performance

To address potential numerical instability arising from the big-M approach, sensitivity analyses for constant M are conducted based on the theoretical lower bound. The specific candidate values of M and the corresponding computational performance are presented in Supplementary Material A Table SAI. The results demonstrate that selecting the tightest valid bound (i.e., $M=-20$) yields the highest computational efficiency for both MGFOR construction and the model solution of MG layer, improving the solution speed while ensuring numerical stability. It is also worth noting that, due to the small number of binary variables and low combinatorial complexity in the subproblems, the branch-and-bound tree terminates at the root node under default solver settings, where an optimal integer-feasible solution is directly obtained.

B. Characterization of MGFOR

Based on the proposed MGFOR model, MGFOR of MG_2 (denoted as $MGFOR_2$) during typical periods as shown in Fig. 2, is selected for analysis to investigate its characteristics.

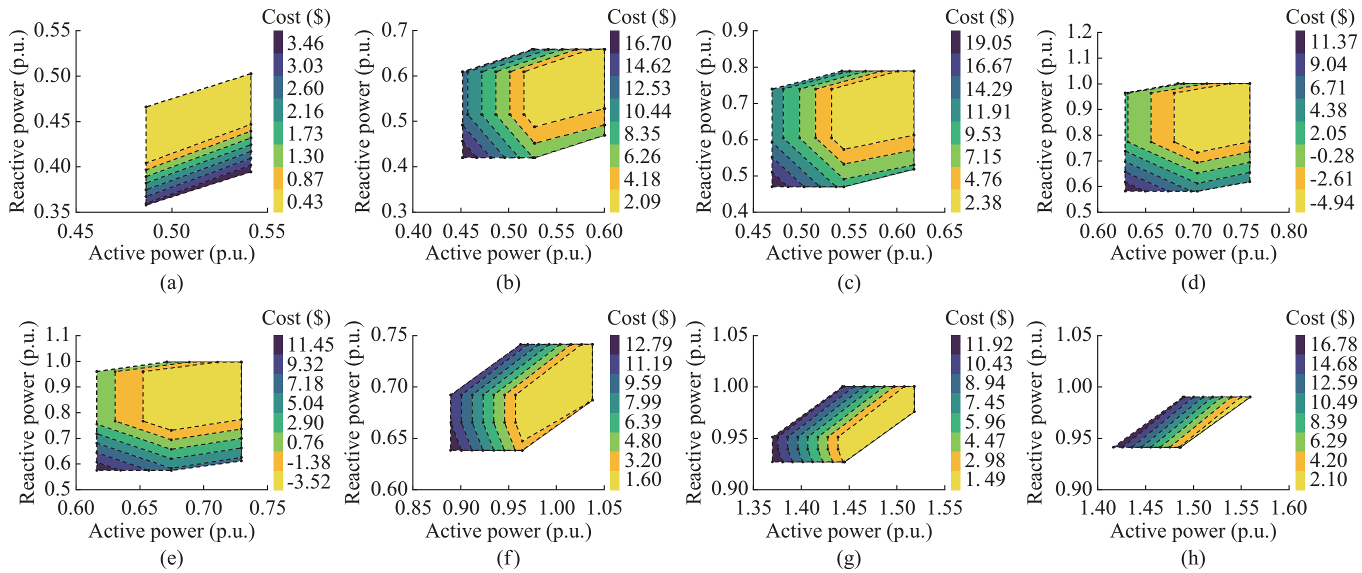

Fig. 2. $MGFOR_2$ during typical periods. (a) 07:00-08:00. (b) 08:00-09:00. (c) 09:00-10:00. (d) 11:00-12:00. (e) 12:00-13:00. (f) 17:00-18:00. (g) 18:00-19:00. (h) 19:00-20:00.

On a single-period surface, as ARC increases, the area of $MGFOR_2$ expands, reflecting the enhanced adjustability of MG_2. The boundary corresponding to the maximum ARC is solely constrained by internal operation limits, representing a physical boundary. In contrast, boundaries at lower ARC tiers are restricted by economic considerations, forming economic-physical boundaries.

Due to variations in marginal adjustment cost, adjustable capacity, and dispatch rules among different FRs, $MGFOR_2$ exhibits non-uniform expansion across dimensions as ARC increases. From 07:00 to 08:00, limited ESS capacity and weak reactive power regulation from distributed PV unit result in reduced flexibility, with $MGFOR_2$ primarily expanding downward along the reactive power axis, indicating decreased reactive power demand. Between 11:00 and 12:00, the availability of ESS charging capacity and high PV output lead to greater flexibility, with the region expanding toward the lower-left quadrant, reflecting simultaneous reductions in active and reactive power demands. From 18:00 to 19:00, $MGFOR_2$ shifts leftward along the active power axis due to ESS discharging and constrained reactive power support from PV, indicating a reduction in active power demand.

Moreover, the continuous evolution of $MGFOR_2$ reveals the temporal coupling characteristic of the flexible operation region, wherein the current dispatch strategy of FRs directly affects the future flexibility of MG_2. Specifically, the power actions of ESS and the response capabilities of FL during the present period alter the availability of FRs during subsequent periods, which is reflected in the changing area of $MGFOR_2$. This characteristic underscores a critical consideration in real-time dispatch: short-term economic benefits must be weighed against long-term flexibility to prevent global flexibility deficits caused by locally optimal decisions.

C. Analysis of Coordinated Dispatch Result

Given the temporal characteristic of MGFOR, appropriately setting the reference voltage at the PCC is crucial to ensure global flexibility. In this paper, to balance control simplicity and operation practicality, the reference voltage at each PCC is set based on the voltage profile from the HD framework, which is adjusted per period to adapt load and PV conditions.

1) Analysis of Operation Cost

The HD framework typically overlooks the active responsiveness of FRs within MG and adheres to a bottom-up dispatch logic. Each MG independently performs local optimization and submits its dispatch scheme to DN, which then conducts global optimization based on these inputs [29]. In contrast, the proposed CD framework integrates MG flexibility into the decision-making process of DN. The comparison of operation costs for HD framework and proposed CD framework is provided in Table II.

TABLE II
COMPARISON OF OPERATION COSTS FOR HD FRAMEWORK AND PROPOSED CD FRAMEWORK

Frame-work	Total operation cost (\$)	Operation cost of DN (\$)	Operation cost of MG_1 (\$)	Operation cost of MG_2 (\$)
HD	13812.0	10685.4	313.2	2813.4
Proposed	13512.7	10432.0	295.9	2784.8

Compared with the HD framework, the proposed CD framework effectively reduces operation costs for both DN and MG. By optimally allocating FRs within MGs, DN effectively avoids load curtailment during peak-demand periods in the evening, while MGs benefit from lower electricity purchase expenses. Consequently, the total operation cost is reduced by approximately 2.2%, reflecting improved economic efficiency.

2) Analysis of Active and Reactive Power Flexibilities

The distribution of active and reactive power flexibilities for MG_1 and MG_2 is illustrated in Fig. 3.

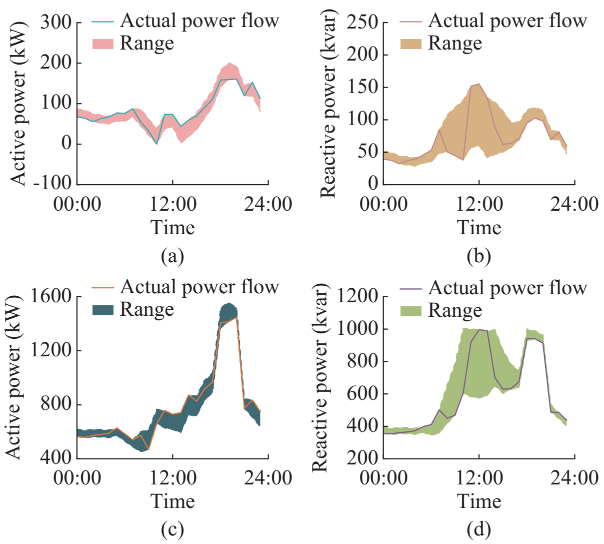

Fig. 3. Distribution of active and reactive power flexibilities for MG_1 and MG_2. (a) Active power flexibility of MG_1. (b) Reactive power flexibility of MG_1. (c) Active power flexibility of MG_2. (d) Reactive power flexibility of MG_2.

The active power flexibility remains relatively stable across different periods due to the balanced contribution from ESSs and HVAC systems. In contrast, reactive power flexibility peaks at noon, coinciding with the maximum PV output. The actual power flow on the tie line shows that both MGs increase their demand during off-peak-demand periods and reduce it during peak-demand periods, effectively achieving demand-side peak shaving and valley filling. This behavior contributes to improved system safety and operation stability. Moreover, as MGs offer multiple regulation levels, DN does not always operate at the flexibility boundary. Preserving a portion of the adjustable capacity of MG helps prevent the depletion of future flexibility, thereby supporting the long-term economic performance of the system.

3) Analysis of Equipment Dispatch

The dispatch strategies of the ESSs and HVAC units are presented in Fig. 4. The ESSs operate through a bi-directional charging or discharging mechanism. Charging primarily occurs during 11:00-13:00 when PV output is abundant, and during 22:00-24:00 when system load is minimal, which supports PV energy absorption and helps smooth load fluctuations. Discharging is concentrated during 08:00-11:00, 13:00-15:00, 18:00-19:00, and 19:00-21:00, thereby reducing electricity purchases from the upper grid during peak-demand periods and enhancing the operation economy. However, differences are observed in the discharging profiles of DN-side and MG-side ESSs. DN-side ESS dispatches follow peak-valley dispatch rules, while MG-side ESS is also subject to DN dispatch instructions. In this case study, the discharging capacity of MG-side ESS is utilized in the DN dispatch during the peak-demand periods in late evening to prevent load shedding. Additionally, as the peak-valley electricity price gap widens, the profitability of MG-side ESS further increases.

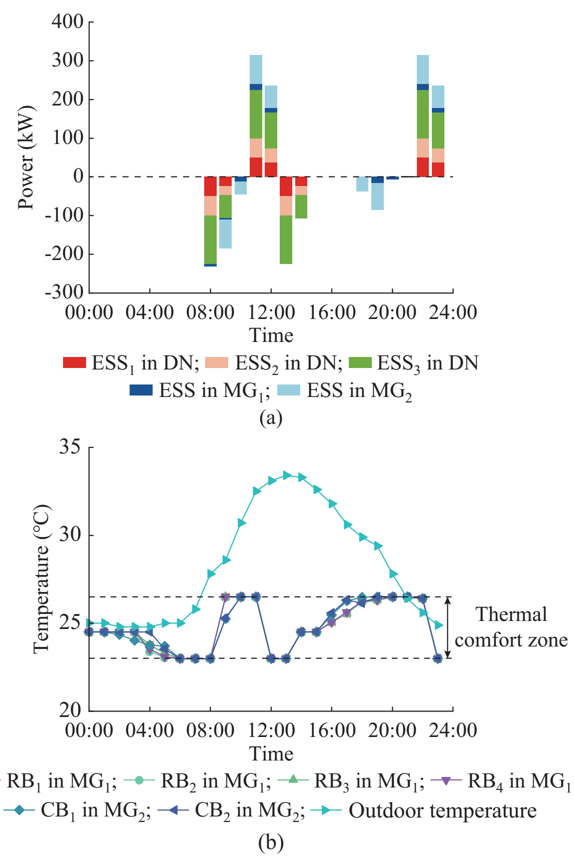

Fig. 4. Dispatch strategies of ESSs and HVAC units. (a) Dispatch strategy of ESSs. (b) Dispatch strategy of HVAC units.

The HVAC load is regulated based on the peak-valley time division. While maintaining user thermal comfort, HVAC units increase power consumption during off-peak-demand periods, resulting in a slight decrease in indoor temperature, reduced consumption during peak-demand periods, and a slight temperature rise. Notably, HVAC units provide 65% of the total active power regulation of MG during critical peak-demand periods in the evening, demonstrating the essential role of FL in grid support. Additionally, engaging HVAC units in DR participation has also contributed to improving the overall economic performance of MG operation.

Distributed PV units, constrained by their operation characteristics, supply reactive power compensation only during periods with active power generation. The specific operation profile illustrating this characteristic is provided in Supplementary Material A Fig. SA2. During morning and afternoon, PVs inject reactive power to locally compensate for demand, thereby reducing long-distance reactive power transmission and associated line losses. However, at noon when PV output peaks and the risk of voltage exceeding the upper limit increases, PVs absorb reactive power to mitigate voltage rise within DN.

D. Effectiveness Analysis of Active Support Capability of MG

To demonstrate the active support capability of MGs, simulation results comparing node voltage profiles and network losses under two dispatch frameworks are presented. These comparisons validate the effectiveness of the proposed CD framework in mitigating voltage fluctuations and reducing line losses by leveraging the FRs within MGs.

1) Node Voltage

The node voltage distribution in DN under both dispatch frameworks is illustrated in Fig. 5, where the blue part indicates the proposed CD framework, and the purple part indicates the HD framework.

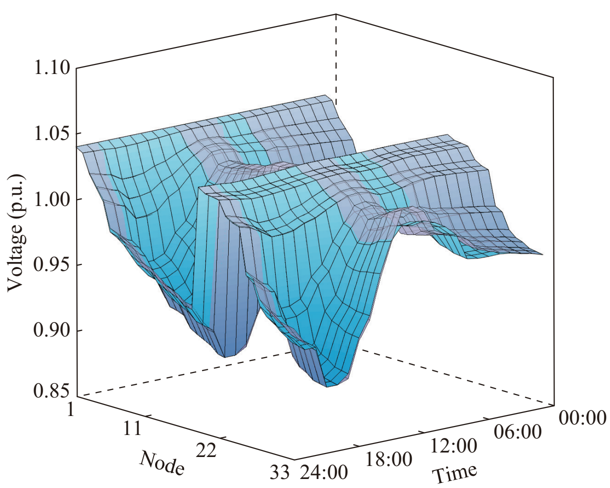

Fig. 5. Node voltage distribution in DN under both dispatch frameworks.

Simulation results indicate that significant voltage fluctuations occur during the peak-demand periods of PV generation in the midday and peak-load periods in the evening, increasing the risk of voltage violations. By implementing the proposed CD framework, MG uses internal FRs to actively support voltage regulation needs, effectively mitigating voltage deviations. Specifically, the voltage security margin at end-of-feeder nodes in the midday achieves a maximum relative improvement of 56.46%. Although the adjustable capacity of MG is relatively constrained in the evening, resulting in minimal improvement to voltage security margins, the system consistently maintains secure operation without violations.

2) Network Loss

The detailed distribution of network losses under both dispatch frameworks is presented in Supplementary Material A Table SAII. Although the proposed CD framework results in a relative increase of 4.37% in network losses—attributable to elevated HVAC demand during off-peak-demand periods and reactive power support from PV—the associated cost is offset by user-side DR benefits.

Consequently, the overall system operation efficiency is improved. This trade-off is considered acceptable and does not constitute a drawback of the proposed CD framework. A full multi-objective Pareto analysis could be explored in future work for systems where loss minimization is a primary concern.

E. Sensitivity Analysis

Additionally, the number of ARC tiers and the operation mode of equipment are adjusted to evaluate the synergistic effect between DN and MG.

1) Number of ARC Tiers

The comparison of operation costs under different numbers of ARC tiers is presented in Table III. Simulation results indicate that, because DN tends to operate along the physical boundaries of MGFOR to dispatch the operation state of MG, the need for intermediate ARC tiers is limited. Consequently, the influence of the number of ARC tiers on total operation cost is minimal. This finding confirms that, in certain scenarios, simplifying the number of ARC tiers can effectively balance operation cost and computational efficiency. However, in DNs with high renewable energy penetration of stringent voltage regulation requirements, the relationship between regulation granularity and control accuracy may alter this conclusion.

TABLE III
COMPARISON OF OPERATION COSTS UNDER DIFFERENT NUMBERS OF ARC TIERS

Number of ARC tiers	Total operation cost ($)	Operation cost of DN ($)	Operation cost of MG_1 ($)	Operation cost of MG_2 ($)
4	13520.2	10436.8	295.5	2787.8
6	13512.9	10434.0	295.9	2783.1
8	13512.7	10432.0	295.9	2784.8

2) Operation Mode of Equipment

The flexibility supply capability of MG is influenced by different operation modes of its internal FR devices, which in turn affects MG support to DN. In particular, the impact of enabling the reactive power support mode in distributed PV unit is assessed by analyzing voltage quality differences across DN nodes. The detailed comparisons of operation modes and the corresponding voltage magnitudes at key DN nodes are presented in Supplementary Material Fig. SA3. It is observed that by activating the reactive power compensation function of the distributed PV unit in the evening, the voltage profile is effectively improved, and the overall voltage stability margin of the system is enhanced, especially under high line loading conditions.

F. Performance Analysis Under Extreme High-temperature Condition

To evaluate the robustness of the proposed CD framework under stress conditions, we simulate an extreme high-temperature day, during which PV output is reduced due to thermal derating, while loads increase significantly. Under this condition, the risk of daytime overvoltage is mitigated, but the undervoltage and load curtailment in the evening become critical concerns.

Simulation results show that the system experiences load shedding during the peak-demand periods in the evening under both the HD framework and proposed CD framework due to insufficient flexibility. However, by leveraging MGFOR to concentrate flexible capacity—particularly the reactive power compensation capacity from distributed PV units—during the critical peak-demand periods in the evening, the proposed CD framework enables the 87.52% reduction in load shedding while simultaneously lowering the total operation cost by 9.94%, relative to the HD framework. This confirms that the benefits of the proposed CD framework not only persist but are amplified under extreme operation conditions.

V. Conclusion

To address the need for coordinated interaction between DN and MG, a coordinated dispatch framework of DN and MG via MGFOR is presented in this paper. By applying the convex-hull fitting approach, the MGFOR model accurately characterizes the regulation capability of MG under ARC constraints, which contributes to providing effective support for enhancing both economic efficiency and voltage security in the co-optimization of DN and MG. Simulation results demonstrate that, by leveraging intra-MG FRs, the proposed CD framework effectively prevents emergency load shedding to achieve 2.2% operation cost reductions while enhancing voltage safety margins at distribution feeder terminals by up to 56.46% during peak-demand periods of PV at noon. Furthermore, the influence of ARC tier granularity on coordination performance has been assessed. It is shown that higher ARC tier granularity enhances adjustment precision but increases computational complexity. In addition, the operation mode of FR devices affects MG flexibility; notably, enabling reactive power support in distributed PV units in the evening improves voltage levels at critical nodes in DN.

We provide decision support for the coordinated dispatch of DN and MG based on quantified assessment of MG flexibility. This offers valuable insights for optimizing FR allocation, evaluating real-time operation state of MG, and designing privacy-preserving coordinated framework. However, wider implementation faces challenges including: the absence of standardized cost accounting for FR dispatch; computational delays in real-time MGFOR due to inadequate computational resources; and the lack of standardized communication protocols for data exchange between DN and MG.

Future work will explore the possibility of embedding dynamic voltage references informed by MGFOR geometry under source-load uncertainties to enhance coordination adaptability. Additionally, developing a multi-interval MGFOR model is identified as a critical future research direction.

References

[1] IEA. (2024, Oct.). World energy outlook 2024. [Online]. Available: https://www.iea.org/reports/world-energy-outlook-2024

[2] H. Sheng, C. Wang, B. Li *et al*., "Multi-timescale active distribution network scheduling considering demand response and user comprehensive satisfaction," *IEEE Transactions on Industry Applications*, vol. 57, no. 3, pp. 1995-2005, May 2021.

[3] J. Hu, Y. Shan, Y. Yang *et al*., "Economic model predictive control for microgrid optimization: a review," *IEEE Transactions on Smart Grid*, vol. 15, no. 1, pp. 472-484, Jan. 2024.

[4] M. Alipour, G. B. Gharehpetian, R. AhmadiAhangar *et al*., "Cost-aware flexibility evaluation for microgrids," *Journal of Modern Power Systems and Clean Energy*, vol. 13, no. 3, pp. 1003-1013, May 2025.

[5] H. Wu, Z. Xu, M. Wang *et al*., "Full-model-free adaptive graph deep deterministic policy gradient model for multi-terminal soft open point voltage control in distribution systems," *Journal of Modern Power Systems and Clean Energy*, vol. 12, no. 6, pp. 1893-1904, Nov. 2024.

[6] R. B. Navesi, A. F. Naghibi, H. Zafarani *et al*., "Reliable operation of reconfigurable smart distribution network with real-time pricing-based demand response," *Electric Power Systems Research*, vol. 241, p. 111341, Apr. 2025.

[7] M. Norouzi, J. Aghaei, T. Niknam *et al*., "Risk-averse and flexi-intelligent scheduling of microgrids based on hybrid Boltzmann machines and cascade neural network forecasting," *Applied Energy*, vol. 348, p. 121573, Jan. 2023.

[8] X. Xue, J. Fang, X. Ai *et al*., "A fully distributed ADP algorithm for real-time economic dispatch of microgrid," *IEEE Transactions on Smart Grid*, vol. 15, no. 1, pp. 513-528, Jan. 2024.

[9] Y. Jia, P. Wen, Y. Yan *et al*., "Joint operation and transaction mode of rural multi microgrid and distribution network," *IEEE Access*, vol. 9, pp. 14409-14421, Jan. 2021.

[10] Y. Fu, Z. Zhang, Z. Li *et al*., "Energy management for hybrid AC/DC distribution system with microgrid clusters using non-cooperative game theory and robust optimization," *IEEE Transactions on Smart Grid*, vol. 11, no. 2, pp. 1510-1525, Mar. 2020.

[11] H. Quan, K. Utkarsh, and D. Srinivasan, "A distributed dual-optimization framework for ancillary-service coordination between MV microgrids and LV distribution networks," *IEEE Systems Journal*, vol. 17, no. 1, pp. 212-223, Mar. 2023.

[12] A. Mallick, A. Mishra, A. R. Hota *et al*., "Distributed coordination of multi-microgrids in active distribution networks for provisioning ancillary services," *IEEE Systems Journal*, vol. 18, no. 3, pp. 1492-1503, Sept. 2024.

[13] Q. Wu, Z. Liu, M. Zhang *et al*., "Economic optimal dispatch of multi-agent microgrids based on analytical target cascading," in *Proceedings of International Conference on Energy, Power and Electrical Engineering*, Wuhan, China, Jun. 2023, pp. 918-922.

[14] M. A. Igder and X. Liang, "Service restoration using deep reinforcement learning and dynamic microgrid formation in distribution networks," *IEEE Transactions on Industry Applications*, vol. 59, no. 5, pp. 5453-5472, Sept. 2023.

[15] S. Zheng, K. Liao, J. Yang *et al*., "Optimal scheduling of distribution network with autonomous microgrids: frequency security constraints and uncertainties," *IEEE Transactions on Sustainable Energy*, vol. 14, no. 1, pp. 613-629, Jan. 2023.

[16] X. Yang, Z. Song, J. Wen *et al*., "Network-constrained transactive control for multi-microgrids-based distribution networks with soft open points," *IEEE Transactions on Sustainable Energy*, vol. 14, no. 3, pp. 1769-1783, Jul. 2023.

[17] M. Farrokhi, M. Fotuhi-Firuzabad, A. Safdarian *et al*., "Cooperative operational planning of interruptible load contracts for enhancing performance reliability of multi-microgrid power distribution systems," *IEEE Access*, vol. 12, pp. 121610-121623, Aug. 2024.

[18] M. Dabbaghjamanesh, S. Senemmar, and J. Zhang, "Resilient distribution networks considering mobile marine microgrids: a synergistic network approach," *IEEE Transactions on Industrial Informatics*, vol. 17, no. 8, pp. 5742-5750, Aug. 2021.

[19] M. E. Parast, M. H. Nazari, and S. H. Hosseinian, "Resilience improvement of distribution networks using a two-stage stochastic multi-objective programming via microgrids optimal performance," *IEEE Access*, vol. 9, pp. 102930-102952, Jul. 2021.

[20] Z. Tan, Z. Yan, H. Zhong *et al*., "Non-iterative solution for coordinated optimal dispatch via equivalent projection–part II: method and applications," *IEEE Transactions on Power Systems*, vol. 39, no. 1, pp. 899-908, Jan. 2024.

[21] P. Hao, C. Huang, C. Wang *et al*., "Non-iterative coordinated optimal dispatch of distribution system and microgrids via fast approximation equivalent projection," *IEEE Transactions on Smart Grid*, vol. 16, no. 5, pp. 3934-3948, Sept. 2025.

[22] S. Chen, Z. Wei, G. Sun *et al*., "Convex hull based robust security region for electricity-gas integrated energy systems," *IEEE Transactions on Power Systems*, vol. 34, no. 3, pp. 1740-1748, May 2019.

[23] H. Früh, S. Müller, D. Contreras *et al*., "Coordinated vertical provision of flexibility from distribution systems," *IEEE Transactions on Power Systems*, vol. 38, no. 2, pp. 1834-1844, Mar. 2023.

[24] S. Li and W. Wu, "Adaptive voltage control to coordinate multiple PV inverters as a cluster," *IEEE Transactions on Smart Grid*, vol. 15, no. 6, pp. 5526-5538, Nov. 2024.

[25] M. Farivar and S. H. Low, "Branch flow model: relaxations and convexification–part I," *IEEE Transactions on Power Systems*, vol. 28, no. 3, pp. 2554-2564, Aug. 2013.

[26] D. A. Contreras and K. Rudion, "Improved assessment of the flexibility range of distribution grids using linear optimization," in *Proceedings of Power Systems Computation Conference*, Dublin, Ireland, Aug. 2018, pp. 1-7.

[27] M. Xie, X. Ji, S. Ke *et al*., "Autonomous optimized economic dispatch of active distribution power system with multi-microgrids based on analytical target cascading theory," *Proceedings of the CSEE*, vol. 37, no. 17, pp. 4911-4921, Sept. 2017.

[28] P. Liu. (2025, May). Supplementary dataset. [Online]. Available: https://doi.org/10.6084/m9.figshare.30610289.v1

[29] I. I. Picioroaga, A. Tudose, D. O. Sidea *et al*., "Two-level scheduling optimization of multi-microgrids operation in smart distribution networks," in *Proceedings of International Conference and Exposition on Electrical and Power Engineering*, Iasi, Romania, Aug. 2020, pp. 407-412.

Zhinong Wei received the B.S. degree from Hefei University of Technology, Hefei, China, in 1984, the M.S. degree from Southeast University, Nanjing, China, in 1987, and the Ph.D. degree from Hohai University, Nanjing, China, in 2004. He is currently a Professor of electrical engineering with the School of Electrical and Power Engineering, Hohai University. His research interests include integrated energy system, power system state estimation, smart distribution system, and integration of distributed generation into electric power system.

Peng Liu received the B.S. degree from the College of Energy and Electrical Engineering, Hohai University, Nanjing, China, in 2023. He is currently pursuing the M.S. degree with the School of Electrical and Power Engineering, Hohai University. His research interests include optimal dispatch of distribution network.

Sheng Chen received the B.S. and Ph.D. degrees from the School of Electrical and Power Engineering, Hohai University, Nanjing, China, in 2014 and 2019, respectively. From January 2018 to January 2019, he was a Visiting Scholar at The Ohio State University, Columbus, USA. He is currently a Professor with the School of Electrical and Power Engineering, Hohai University. His research interests include integrated energy system and electricity market.

Jingtao Zhao is received the B.S. and M.S. degrees from Hohai University, Nanjing, China, in 2012 and 2017, respectively. He is the Deputy General Manager of Power Distribution/Agricultural Power Branch in NARI Technology Development Co., Ltd., Nanjing, China. His research interests include distribution network automation, AC/DC hybrid distribution network, distributed generation, and microgrid.

Shu Zheng is an Engineer in NARI Technology Development Co., Ltd., Nanjing, China. Her research interests include distribution network automation and AC/DC hybrid distribution network.

Guoqiang Sun received the B.S., M.S., and Ph.D. degrees in electrical engineering from Hohai University, Nanjing, China, in 2001, 2005, and 2010, respectively. From 2015 to 2016, he was a Visiting Scholar with North Carolina State University, Raleigh, USA. He is currently a Professor with the School of Electrical and Power Engineering, Hohai University. His research interests include power system analysis, economic dispatch, and optimal control of integrated energy system.